Journal of Magnetism and Magnetic Materials 401 (2016) 394–405

Contents lists available at ScienceDirect

Journal of Magnetism and Magnetic Materials

journal homepage: www.elsevier.com/locate/jmmm

Nonlinear nano-scale localized breather modes in a discrete weak ferromagnetic spin lattice

L. Kavitha [a,b,c,*], E. Parasuraman [d,f], D. Gopi [e,f], A. Prabhu [d], Rodrigo A. Vicencio [g,b]

[a] Department of Physics, School of Basic and Applied Sciences, Central University of Tamil Nadu (CUTN), Thiruvarur 610 101, Tamil Nadu, India
[b] Max-Planck Institute for the Physics of Complex Systems, Dresden, Germany
[c] The Abdus Salam International Centre for Theoretical Physics, Trieste, Italy
[d] Department of Physics, Periyar University, Salem 636 011, Tamil Nadu, India
[e] Department of Chemistry, Periyar University, Salem 636 011, Tamil Nadu, India
[f] Center for Nanoscience and Nanotechnology, Periyar University, Salem 636 011, Tamil Nadu, India
[g] Departamento de Física and MSI-Nucleus on Advanced Optics, Center for Optics and Photonics (CEFOP), Facultad de Ciencias, Universidad de Chile, Santiago 7800003, Chile

ARTICLE INFO

Article history:
Received 17 December 2014
Received in revised form
2 October 2015
Accepted 8 October 2015
Available online 23 October 2015

Keywords:
Soliton
Exchange interactions
Localized modes
Spin dynamics

ABSTRACT

We investigate the propagation dynamics of highly localized discrete breather modes in a weak ferromagnetic spin lattice with on-site easy axis anisotropy due to crystal field effect. We derive the discrete nonlinear equation of motion by employing boson mappings and p-representation. We explore the onset of modulational instability both analytically in the framework of linear stability analysis and numerically by means of molecular dynamics (MD) simulations, and a perfect agreement was demonstrated. It is also explored that how the antisymmetric nature of the canted ferromagnetic lattice supports highly localized discrete breather (DBs) modes as shown in the stability/instability windows. The energy exchange between low amplitude discrete breathers favours the growth of higher amplitude DBs, resulting eventually in the formation of few long-lived high amplitude DBs.

1. Introduction

The study of nonlinear dynamics in discrete spin systems has recently attracted special attention owing to novel physics and possible interesting applications [1–4]. It is also well known that models describing microscopic phenomena in spin lattices are inherently discrete and this discreteness effect may drastically modify the nonlinear dynamics and properties of spatially localized models [4–6]. Both nonlinearity and lattice discreteness have played important roles in many branches of condensed matter physics and spin dynamics [7]. An important advance in dealing with nonlinearity in condensed matter physics has been the introduction of the soliton as a new type of elementary excitations. One-dimensional classical continuum Heisenberg ferromagnetic spin chains with different magnetic interactions such as bilinear and biquadratic exchange interactions, weak ferromagnetic interaction, octupole–dipole interaction, site and spin dependent interactions, interaction with external magnetic field and anisotropic interactions act as an interesting class of nonlinear dynamical systems exhibiting a rich variety of integrability properties and soliton spin excitations [8–20]. In addition to the dominant magnetic interactions which include integrable spin models with soliton spin excitations, there exist certain magnetic interactions that are less spoken about in the literature of nonlinear dynamics due to the mathematical complexity of their representations in the Hamiltonian and in the governing dynamical equations [8–10]. Notable among them is the Dzyaloshinsky–Moriya (DM) interaction, which is essentially an antisymmetric spin coupling interaction that occurs when the symmetry around the magnetic ions is not high enough, thus leading to the mechanism of weak ferromagnetism (see Fig. 1). Despite being small, this DM interaction is often present in the models of many low-dimensional magnetic materials and generate many spectacular features [21,22]. It was realized by Dzyaloshinsky [23] that the appearance of weak ferromagnetism in some antiferromagnetic materials can be explained solely on the grounds of symmetry. In other words, if the symmetry of the purely antiferromagnetic state is such that the appearance of a small magnetization $\vec{M}$ does not lead to a further symmetry lowering, then any microscopic mechanism which favours a nonzero magnetization, even if it is rather weak will lead to $\vec{M} \neq 0$. It was later shown by Moriya [24,25] that an invariant of the required form can result from an antisymmetric microscopic

* Corresponding author at: Department of Physics, School of Basic and Applied Sciences, Central University of Tamil Nadu (CUTN), Thiruvarur 610 101, Tamil Nadu, India. Fax: +91 4366 225312.
E-mail address: louiskavitha@yahoo.co.in (L. Kavitha).

http://dx.doi.org/10.1016/j.jmmm.2015.10.021
0304-8853/

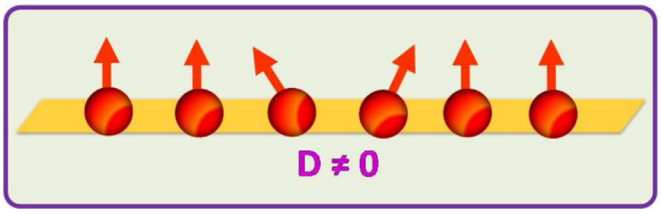

Fig. 1. Dzyaloshinsky–Moriya interaction with slight canting of the magnetic moments.

coupling between two localized magnetic moments $\vec{S}_i$ and $\vec{S}_j$

$$H^{DM} = \vec{D}_i \cdot (\vec{S}_i \times \vec{S}_j), \tag{1}$$

and such an interaction arises from the interplay between super-exchange and spin–orbit coupling. The energy (1) is minimized when the two magnetic moments form a 90° angle, but due to the simultaneous presence of the generally much stronger Heisenberg-type interaction $H^B = J_{ij}\vec{S}_i \cdot \vec{S}_j$, which favours either 0° or 180° angle, the presence of the DM interaction usually leads to a small canting between the interacting moments. Weak ferromagnetic spin chains act as natural candidates for the realization of entanglement basis, and the Heisenberg chain has been used in quantum computation and construction of a quantum computer [26,27].

However, in nonlinear discrete systems, the spatial size of the nonlinear excitations can be comparable to the lattice spacing, hence the discreteness of the underlying physical systems is expected to have a significant effect on the properties of nonlinear excitations [28]. This realization has led to the extensive studies of the features associated with intrinsic localization modes in various nonlinear nonintegrable lattices, and it has been proved to be a conceptual and practical breakthrough [28]. In the literature, these localized excitations are called DBs with the fact that their formation involves no disorder and that they extend over a nano-length scale in the discrete lattice [28]. Discrete breathers or intrinsic localized modes (ILMs) are time periodic and spatially localized excitations that may be produced generically in discrete arrays of weakly coupled nonlinear elements [29]. In addition, the existence of DBs has been postulated theoretically by means of precise numerical analysis in discrete nonlinear lattices [30,31]. Breathers have also been experimentally observed in several diverse systems, including optical wave guides [32], solid state systems [33,34], antiferromagnetic chains [35], Josephson-junction arrays [36], micromechanical oscillators [37,38] and even possibly in myoglobin [39]. The analogy between lattice vibrations and spin waves has generated some studies on intrinsic localized spin waves in semiclassical and classical magnetic models [40–45]. In this context, studies have shown, that the existence of various ILMs is accompanied by an instability of the corresponding nonlinear plane waves [46,47] and the phenomenon of modulational instability (MI) acts as a possible mechanism for the energy localization in discrete lattices and it has been studied in a number of discrete models [48–50]. MI, which refers to the exponential growth of certain modulation side-bands of nonlinear plane waves propagating in a dispersive medium as a result of the interplay between nonlinearity and dispersion, has been studied in various fields [51,52].

In magnetic systems, it has been shown that intrinsic localized spin wave modes (ILSMs) can also occur in perfect but non-integrable magnetic models [53–58]. It has been reported that in the presence of a strong magnetic field perpendicular to the easy-plane, both even-parity and odd-parity ILSMs appear in easy-plane Heisenberg ferromagnetic chains when the strength of single-ion anisotropy exceeds a certain value. It has also been demonstrated numerically that in-band nonlinear localized excitations in easy-plane antiferromagnetic chains can occur and that they are long lived. So far the intrinsic localization of spin waves has been identified only in the Heisenberg spin chain with lower order nearest-neighbour interactions. Thus the existence of DBs in discrete Heisenberg ferromagnet with DM interaction has become an important problem to be investigated urgently. Here we demonstrate that intrinsic localization can occur in an anisotropic weak ferromagnetic discrete spin chains of classical spins coupled ferromagnetically through both nearest-neighbour and antisymmetric spin coupling with DM interaction.

The paper is organized as the following sections. In Section 2, we present the mathematical background of the model for an anisotropic weak ferromagnetic system and construct the equations of motion and derive the discrete nonlinear equation of motion with the aid of Holstein–Primakoff transformation combined with Glauber's coherent state representation. In Section 3, the analytical investigation of the modulational instability of a plane wave propagating in a discrete weak ferromagnetic chain is presented. A linear stability analysis will be carried out to predict under what conditions nonlinear localized modes will occur. In Section 4, we perform molecular dynamics simulations in order to analyse the long time behaviour of the system and how energy is redistributed in a weak ferromagnetic spin chain. We discuss about the localization and the energy density distribution among the localized modes in Section 5 and also we demonstrate the possible existence of discrete breather localized modes. Finally, we perform the stability analysis in Section 6 and conclude our results in Section 7.

2. Mathematical background of weak ferromagnetic spin dynamics

We consider a one-dimensional ferromagnetic chain of N spins which are coupled through both nearest-neighbour and Dzyaloshinsky–Moriya antisymmetric exchange interactions. The Hamiltonian to be examined is

$$H = -\sum_n \Big[J_1 (S_n^x \cdot S_{n+1}^x + S_n^y \cdot S_{n+1}^y) + J_2 (S_n^z \cdot S_{n+1}^z) + J_3 [\vec{D} \cdot (\vec{S}_n \times \vec{S}_{n+1})] - A (S_n^z)^2 \Big], \tag{2}$$

where $\vec{S}_n = (S_n^x, S_n^y, S_n^z)$ represents the spin angular momentum operator at the lattice site n and $\vec{D} = (D^x, D^y, D^z)$ is the Dzyaloshinsky vector. J_1 represents the bilinear spin–spin coupling in the $(S^x$–$S^y)$ plane and J_2 corresponds to the neighbouring bilinear spin–spin coupling along the S^z direction. The term proportional to J_3 corresponds to the D–M, antisymmetric weak spin coupling. The parameter J_3 characterize the Dzyaloshinsky–Moriya (DM) exchange interaction which is proportional to the vector product of interacting spins and is allowed by symmetry in noncentric crystal structures. This DM interaction is of interest in its own right and is known to be the cause of weak ferromagnetism in certain materials such as Hematite α–Fe_2O_3 [24]. This interaction is also found to enhance the fluctuation of the spin components in the plane perpendicular to $\vec{D}$. The vector $\vec{D}$ denotes the intensity of DM interaction imposed along the chain. To understand what is going on, we first note that for two spins $\vec{S}_1$ and $\vec{S}_2$, interacting via isotropic exchange and the DM term, the interaction energy is minimized at $-\sqrt{J^2 + D^2 S^2}$, when both spins $\vec{S}_1$ and $\vec{S}_2$ are perpendicular to $\vec{D}$ in the absence of an external magnetic field. As shown by Moriya, the cross-product term $\vec{D}_n \cdot (\vec{S}_n \times \vec{S}_{n+1})$ originates from spin-flop hopping, which made the possible existence of

spin-orbit interactions resulting in a canted spin system. The parameter A characterizes the strength of the crystal field anisotropy along the easy axis of magnetization.

For treating the problem semiclassically, we employ the Holstein–Primakoff transformation [59] for the spin operators in terms of boson operators a_n, $a_n^\dagger$ and recast the dimensionless Hamiltonian as follows:

$$\begin{aligned}
H = &-1/2\sum_i \{J_1\Big[2\epsilon^2[a_n^\dagger a_{n+1} + a_n a_{n+1}^\dagger] \\
&- \frac{\epsilon^4}{2}[a_n^\dagger a_n^\dagger a_n a_{n+1} + a_n^\dagger a_{n+1}^\dagger a_{n+1} a_{n+1} + a_n^\dagger a_n a_n a_{n+1}^\dagger \\
&+ a_n a_{n+1}^\dagger a_{n+1}^\dagger a_{n+1}] + \frac{\epsilon^6}{16}[2a_n^\dagger a_n^\dagger a_n a_{n+1}^\dagger a_{n+1} a_{n+1} \\
&- a_n^\dagger a_n^\dagger a_n a_n^\dagger a_n a_{n+1} - a_n^\dagger a_{n+1}^\dagger a_{n+1} a_{n+1}^\dagger a_{n+1} a_{n+1} \\
&+ 2a_n^\dagger a_n a_n a_{n+1}^\dagger a_{n+1}^\dagger a_{n+1} - a_n^\dagger a_n a_n^\dagger a_n a_n a_{n+1} \\
&- a_n a_{n+1}^\dagger a_{n+1}^\dagger a_{n+1} a_{n+1}^\dagger a_{n+1}]\Big] \\
&+ 2J_2\Big[1 - \epsilon^2[a_{n+1}^\dagger a_{n+1} + a_n^\dagger a_n] + \epsilon^4[a_n^\dagger a_n a_{n+1}^\dagger a_{n+1}]\Big] \\
&- iJ_3\Big[\sqrt{2}D^+\Big\{\epsilon[a_{n+1}^\dagger - a_n^\dagger] - \frac{\epsilon^3}{4}[a_{n+1}^\dagger a_{n+1}^\dagger a_{n+1} \\
&+ 4a_{n+1}^\dagger a_n^\dagger a_n - a_n^\dagger a_n^\dagger a_n - 4a_n^\dagger a_{n+1}^\dagger a_{n+1}] \\
&- \frac{\epsilon^5}{32}[a_{n+1}^\dagger a_{n+1}^\dagger a_{n+1} a_{n+1}^\dagger a_{n+1} - 8a_{n+1}^\dagger a_{n+1}^\dagger a_{n+1} a_n^\dagger a_n \\
&- a_n^\dagger a_n^\dagger a_n a_n^\dagger a_n + 8a_n^\dagger a_n^\dagger a_n a_{n+1}^\dagger a_{n+1}]\Big\}\Big] \\
&+ \frac{1}{2}D^-\Big\{\epsilon[a_n - a_{n+1}] - \frac{\epsilon^3}{4}[a_n^\dagger a_n a_n + 4a_n^\dagger a_{n+1}^\dagger a_{n+1} \\
&- a_{n+1}^\dagger a_{n+1} a_{n+1} - 4a_{n+1}^\dagger a_n a_n] \\
&- \frac{\epsilon^5}{32}[a_n^\dagger a_n a_n^\dagger a_n a_n - 8a_n^\dagger a_n a_n a_{n+1}^\dagger a_{n+1} \\
&- a_{n+1}^\dagger a_{n+1} a_{n+1}^\dagger a_{n+1} a_{n+1} + 8a_{n+1}^\dagger a_{n+1} a_{n+1} a_n^\dagger a_n]\Big\} \\
&+ D^z\Big\{2\epsilon^2[a_n^\dagger a_{n+1} - a_n a_{n+1}^\dagger] \\
&- \frac{\epsilon^4}{2}[a_n^\dagger a_n^\dagger a_n a_{n+1} + a_n^\dagger a_{n+1}^\dagger a_{n+1} a_{n+1} - a_n^\dagger a_n a_n a_{n+1}] \\
&- a_n a_{n+1}^\dagger a_{n+1}^\dagger a_{n+1}]\Big\} - 2A\{1 - 2\epsilon^2[a_n^\dagger a_n] + \epsilon^4[a_n^\dagger a_n a_n^\dagger a_n]\} \\
&+ O(\epsilon^6)\}, \qquad (3)
\end{aligned}$$

where $\epsilon = 1/\sqrt{S}$. The dynamics of the spins can be expressed in terms of the Heisenberg equation of motion for the Bose operator a_n:

$$i\hbar\frac{da_n}{dt} = [a_n, H].$$

We then introduce Glauber's coherent-state representation (p-representation) [60] defined by the product of the multimode coherent states $|u\rangle = \prod_n |u_n\rangle$ with $\langle u|u\rangle = 1$. Each component $|u(n)\rangle$ is an eigenstate of the annihilation operator a_n, i.e., $a_n|u\rangle = u_n|u\rangle$, where $|u^*(n)\rangle$ is the coherent-state eigen vector for the operator $a_n^\dagger$ and u_n is the coherent amplitude in this representation. Since coherent states are normalized and overcompleted, the field operators sandwiched by $|u(n)\rangle$ can be represented only with their diagonal elements. The p-representation of nonlinear equation leads

$$\begin{aligned}
&iu_{nt} + 2(u_{n+1} + u_{n-1}) + 4\epsilon^2\gamma|u_n|^2u_n + 2\alpha\epsilon^2(|u_{n+1}|^2 + |u_{n-1}|^2)u_n \\
&- \frac{\epsilon^2}{4}\Big[2(u_{n+1} + u_{n-1})|u_n|^2 + (u_{n+1}^* + u_{n-1}^*)u_n^2 + |u_{n+1}|^2u_{n+1} \\
&+ |u_{n-1}|^2u_{n-1}\Big] - i\beta\Big[(u_{n+1} - u_{n-1}) - \frac{\epsilon^2}{4}\Big[2(u_{n+1} - u_{n-1})|u_n|^2 \\
&- (u_{n+1}^* - u_{n-1}^*)u_n^2 + |u_{n+1}|^2u_{n+1} - |u_{n-1}|^2u_{n-1}\Big]\Big] = 0, \qquad (4)
\end{aligned}$$

where $\alpha = J_2/J_1$, $\beta = J_3D^z/J_1$ and $\gamma = A/J_1$. The above nonlinear differential–difference equation is a generalized discrete nonlinear equation which has not been reported so far. Solving this equation analytically is extremely difficult owing to its high nonlinearity and discreteness. In addition, the discreteness makes the properties of the system periodic, so that due to the interplay between the discreteness and nonlinearity, new types of nonlinear excitations, which are absent in continuum models, may be possible in the present system.

3. Existence conditions for discrete breathers

Wave instabilities are probably the most remarkable nonlinear phenomena that may occur in nature. We study the condition of modulational instability of a constant-amplitude solution of the present model under a plane-wave perturbation and demonstrate the possibility of the localized structures by a linear stability analysis. We find that Eq. (4) allows a constant-amplitude solution

$$u_n(t) = u_0\exp[i(kn - \omega t)], \qquad (5)$$

which exhibits modulational instability leading to a modulation of the solution, where u_0 is the constant amplitude, k and ω represent the wave number and the angular frequency, respectively. Upon substituting the above solution in Eq. (4), yields the following appropriate nonlinear dispersion relation:

$$\omega = 2[\cos k(2 - \epsilon^2u_0^2) + 2\epsilon^2u_0^2(\alpha + \gamma) + \beta\sin k(1 - \epsilon^2u_0^2)]. \qquad (6)$$

Now we study whether the solution is stable against small perturbations by performing a linear stability analysis for which we introduce a perturbed field of the form

$$u_n(t) = (u_0 + \delta u_n(t))\exp[i(kn - \omega t)], \qquad (7)$$

where $\delta u_n(t)$ is a small perturbation of the carrier wave.

Here

$$\delta u_n(t) = u_1\exp[i(Qn - \Omega t)] + u_2^*\exp[-i(Qn - \Omega^* t)],$$

here Q and Ω represent the wave number and the frequency of the linear modulation waves, respectively. Also u_1 and u_2^* are the amplitudes of the carrier wave and assumed to be small when compared to the parameters of the carrier wave and asterisk denotes the complex conjugate. Subsequently upon using $\delta u_n(t)$ and Eqs. (4) and (7), we obtain the following quadratic equation:

$$\Omega^2 + (A^+ - A^-)\Omega + (A^+ + A^-)\omega - \omega^2 - A^+A^- + B^2 = 0, \qquad (8)$$

where

$$\begin{aligned}
\omega &= 2[\cos k(2 - \epsilon^2u_0^2) + 2\epsilon^2u_0^2(\alpha + \gamma) + \beta\sin k(1 - \epsilon^2u_0^2)], \\
A^\pm &= 2[(2 - \epsilon^2u_0^2)\cos(k \pm Q) - \epsilon^2u_0^2\cos k + 2\epsilon^2u_0^2(\alpha + 2\gamma) \\
&\quad + 2\alpha\epsilon^2u_0^2\cos Q + \beta(1 - \epsilon^2u_0^2)\sin(k \pm Q) - \beta\epsilon^2u_0^2\sin k], \\
B &= \epsilon^2u_0^2[4\gamma + (4\alpha - \cos k\beta\sin k)\cos Q - \cos k - \beta\sin k].
\end{aligned}$$

Upon solving for Ω, we obtain the dispersion relation:

$$\Omega = \frac{1}{2}\Big\{ 2\epsilon^2 u_0^2 \sin Q\,(\beta \cos k - \sin k) - 2\beta \cos k \sin Q + \sqrt{4 \sin k \sin Q + \left[X^2 - 4\epsilon^4 u_0^4 Y^2\right]}\Big\}, \tag{9}$$

where,

$$X = 8 \cos k + 4\beta \sin k + \cos(k)\cos(Q)(2\epsilon^2 u_0^2 - 4) + 2\beta \sin(k)\sin(Q)(\epsilon^2 u_0^2 - 1) - 8\epsilon^2 u_0^2(\gamma - \alpha \cos Q),$$

$$Y = \cos k - 4\gamma + \beta \sin k + \cos Q\,[\cos k - 4\alpha + \beta \sin k].$$

The constant amplitude solution (5) is stable if perturbations at any wave number k do not grow with time. This is true as long as frequency Ω is real. From Eq. (9), we find that Ω remains real for any ω provided that $X^2 > Y^2$. However, Ω can become imaginary for $X^2 < Y^2$ and the plane-wave perturbations grow exponentially with time t. The perturbation that grows exponentially with the intensity given by the growth rate or the modulational instability gain $g(\Omega)$ defined by

$$\begin{aligned} g(\Omega) &\equiv Im(\Omega) \\ &\equiv \{4\epsilon^4 u_0^4 \left[\cos k - 4\gamma + \beta \sin k + \cos Q\,[\cos k - 4\alpha + \beta \sin k]\right]^2 \\ &\quad - \Big[8 \cos k + 4\beta \sin k + \cos(k)\cos(Q)(2\epsilon^2 u_0^2 - 4) \\ &\qquad + 2\beta \sin(k)\sin(Q)(\epsilon^2 u_0^2 - 1) \\ &\quad - 8\epsilon^2 u_0^2(\gamma - \alpha \cos Q)\Big]^2 \\ &\quad - 4 \sin k \sin Q\}^{1/2} \end{aligned} \tag{10}$$

where *Im* denotes the imaginary part and existence of localized structures are possible only when the constant-amplitude solution is unstable. The gain equation (10) shows more interesting dependence of Ω on the coupling parameters α, β and γ. Eq. (10) determines the stability and instability of a plane wave with the wave number Q in discrete weak ferromagnetic spin chain and the instability gain spectrum is portrayed for both staggered and unstaggered modes as shown in Figs. 2(a) and (b). Figs. 3–5 depict the regions of stability/instability and the corresponding influence of the coupling parameters α, β and γ are explored pictorially. Fig. 3 portrays the stability/instability regions in the (k, Q) plane by choosing values of $\beta = 1.41$, $\gamma = 0.38$ and for various values of the exchange anisotropic parameter α. In the figures, the dark bluish area corresponds to a region where the nonlinear plane waves are stable with respect to modulation of any wavenumber Q and the region with bright yellowish orange area experiences in which the amplitude of any wave would be expected to suddenly display an exponential growth. From Fig. 3, it is evident from the 2D plots that the domains of modulational instability seems to be enhanced as the value of the exchange anisotropic parameter α increases from $\alpha = 0.41$ to 1.5, thus inducing instability of the propagating plane-wave in the discrete weak ferromagnetic chain. In the 3D plots shown in Fig. 3, the growth rate is increased significantly and the weak ferromagnetic system is driven to highly instable nature of the modulated waves. A similar phenomenon is observed and the domain size of the instability grows further upon an increase in the values of D–M interaction parameter β from $\beta = 0.2$ to 1.2. It is revealed from Fig. 4 that the play-role of the D–M interaction leads to the instability and a subsequent formation of intrinsic localized structures. Surprisingly, an increase in the anisotropy parameter A also leads to the extended domain size of instability more significantly and the corresponding growth rate is depicted in Fig. 5. Thus, in an anisotropic discrete weak ferromagnetic system, the effective presence of the coupling parameters α, β and γ crucially change the stability/instability properties of a propagating plane-wave and subsequently supports the formation of localized structures.

4. Molecular dynamics simulations

Though the modulational instability of nonlinear spin waves have been deduced from the linear stability analysis, such analysis is based only on the linearization around the unperturbed carrier wave. Unfortunately, at large time scale, the analysis neglects additional combination of waves generated through wave mixing processes which become significant if its wave vector falls inside an instability domain. Therefore, in this section, we perform the molecular dynamics (MD) numerical simulations in order to analyse the long time behaviour of the nonlinear spin waves.

The MD simulation is performed with a chain of $N = 256$ spins with periodic boundary conditions, so that the wave vector k is defined modulo 2π in the lattice and chosen in the form $k = 2\pi l/N$ and $Q = 2\pi L/N$, where l and L are integers lower than $N/2$. The initial conditions involve coherently modulated nonlinear spin waves of the form

$$u_n(t) = (u_0 + 0.01 \cos(Qn)) \cos(kn),$$
$$\dot{u}_n(t) = (u_0 + 0.01 \cos(Qn))\omega \sin(kn). \tag{11}$$

The time evolution of a large amplitude zone centre mode is perturbed by random noise in both Fourier and real space

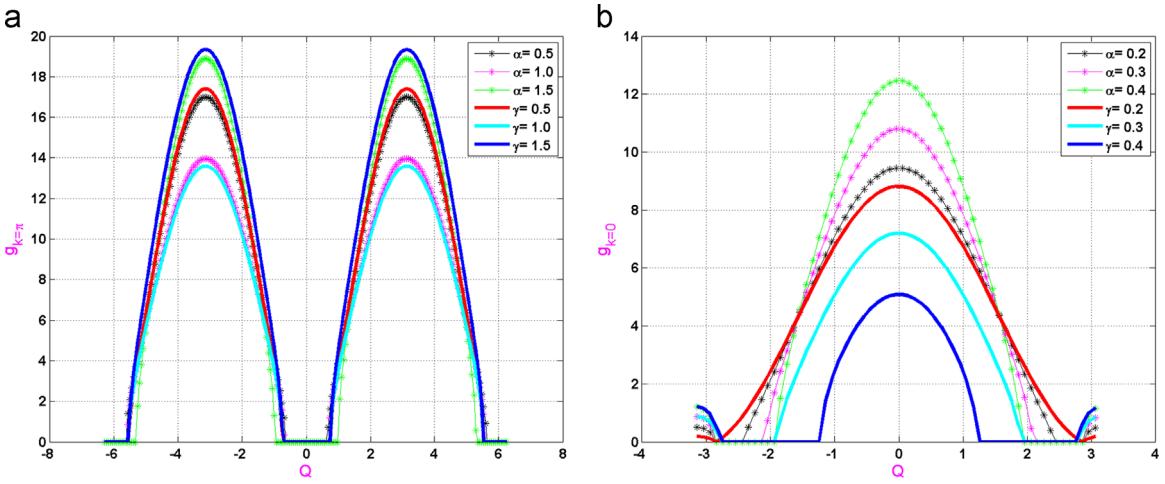

Fig. 2. Instability gain spectrum for the staggered and unstaggered modes. (a) $k = \pi$. (b) $k = 0$.

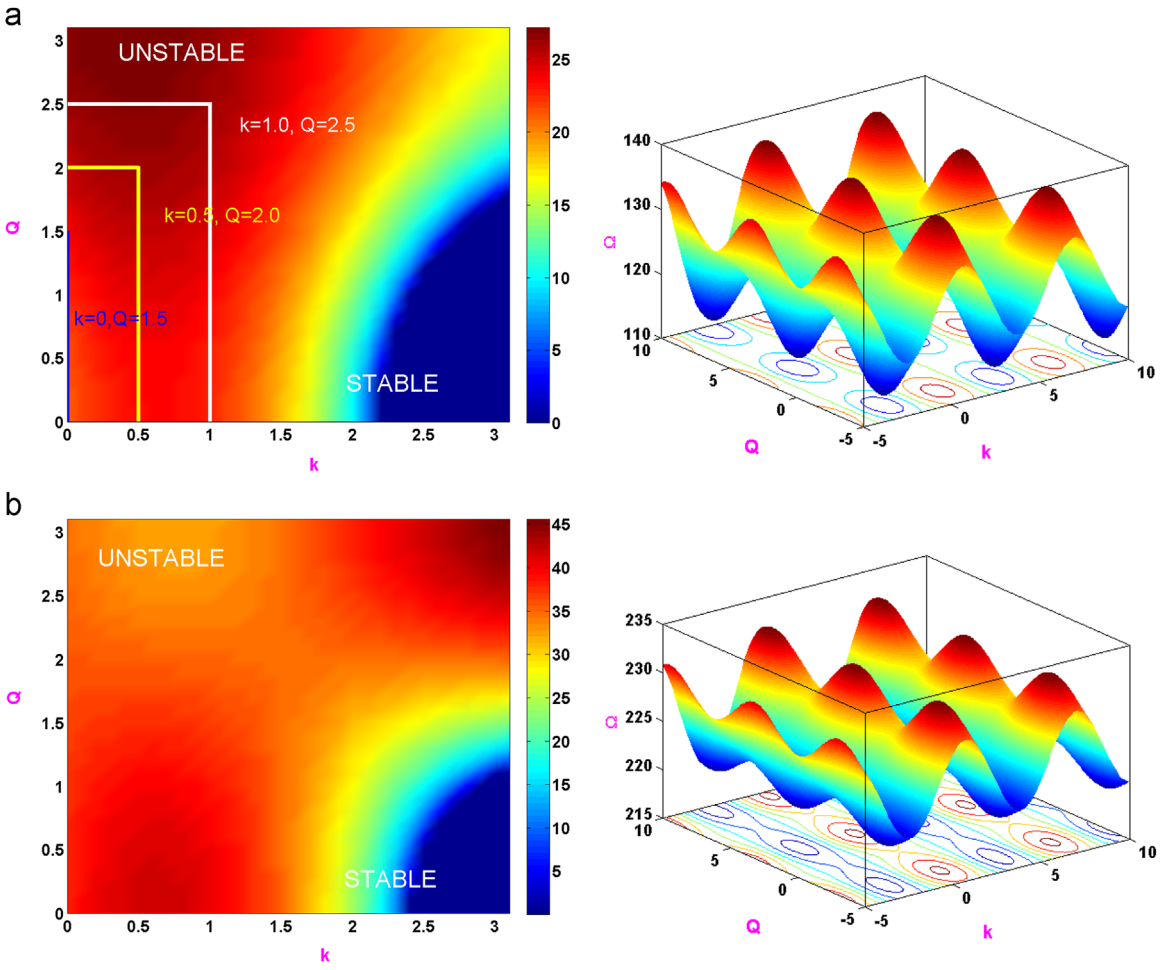

Fig. 3. Left columns: Stability/instability region in the (k, Q) plane. Right columns: MI gain profile for (a) $\alpha=0.41$, (b) $\alpha=1.5$ and on all plots $\beta=1.41$ and $\gamma=0.38$. (For interpretation of the references to color in this figure caption, the reader is referred to the web version of this paper.)

consisting of 256 spins. We study the behaviour of the modulated wave with the help of discrete spatial Fourier transform of the wavefunction:

$$S_p(t) = \sum_{n=0}^{N-1} u_n(t) e^{2i\pi\, ln/N} \quad \text{with } 0 \le l \le N/2. \tag{12}$$

It is worthy to note that $S_p(t) = \langle a_n(t) \rangle$ is the expectation value of the boson operator, which is proportional to the transverse value of $S_n^+ = S_n^x + iS_n^y$ and precessing magnetization thus represents a spin wave-amplitude.

4.1. Stability for short time

We perform molecular dynamics (MD) simulations for the short time period by considering a weak ferromagnetic chain of 256 spins, with periodic boundary conditions in order to monitor the time evolution of individual Fourier components. The growth rate of each individual Fourier component can be obtained by the least square fitting of $|S_p(t)|^2$ over the first few periods during which it is expected to grow at the rate of $g(\Omega)$. The exchange parameters are taken to be $\alpha=0.41$, $\beta=1.41$ and $\gamma=0.38$, and the amplitude $u_0=0.025$. Fig. 6 shows the evolution of a carrier wave with wavevector and modulated by the small amplitude waves (i) $k = 0$, $Q = \pi/2$, (ii) $k = \pi/3$, $Q = 5\pi/6$, respectively, for 100 units of time. From Fig. 6a (i) it is evident that until 30 units of time, none of the $k \pm Q$ satellite side bands display any exponential growth. Even after 30 units of time the exponential growth of satellite side bands stays at the initial stage of instability which obviously can be seen from the log-linear plot of Fig. 6a(i). Further for the increased carrier wave vectors and modulated amplitude waves are shown in Fig. 6a(ii), the satellite sidebands display an exponential growth gradually as evidenced from the corresponding log-linear plots. This can be verified with the stability/instability regions in the (k, Q) plane as depicted in Figs. 3–5. The excellent agreement between them demonstrates that the linear-stability analysis gives quantitatively a correct prediction of the onset of instability. In these figures, even the higher harmonics of the modulation satellite sidebands illustrate the origin of the oscillatory instability leading to a chaotic state of the system.

4.2. Stability for long time

We carry out MD simulations in order to examine the longer time dynamics in the discrete weak ferromagnetic systems which is subjected to MI. The prediction of stability from linear stability analysis does not necessarily rule out the occurrence of instability in the long time evolution of the carrier wave because of the combination of satellite bands neglected there. To illustrate this point, the longer time evolution of the perturbed carrier wave vectors and modulation wave vectors for (i) $k = 0$, $Q = \pi/2$, (ii) $k = \pi/3$, $Q = 5\pi/6$ is depicted in Fig. 6(b). From Fig. 6b(i), it is manifested that until 35 units of time there is no exponential growth and the carrier wave is fairly stable in this regime. However, in Fig. 6b(ii) the carrier wave becomes unstable and generates more and more combination of satellite side

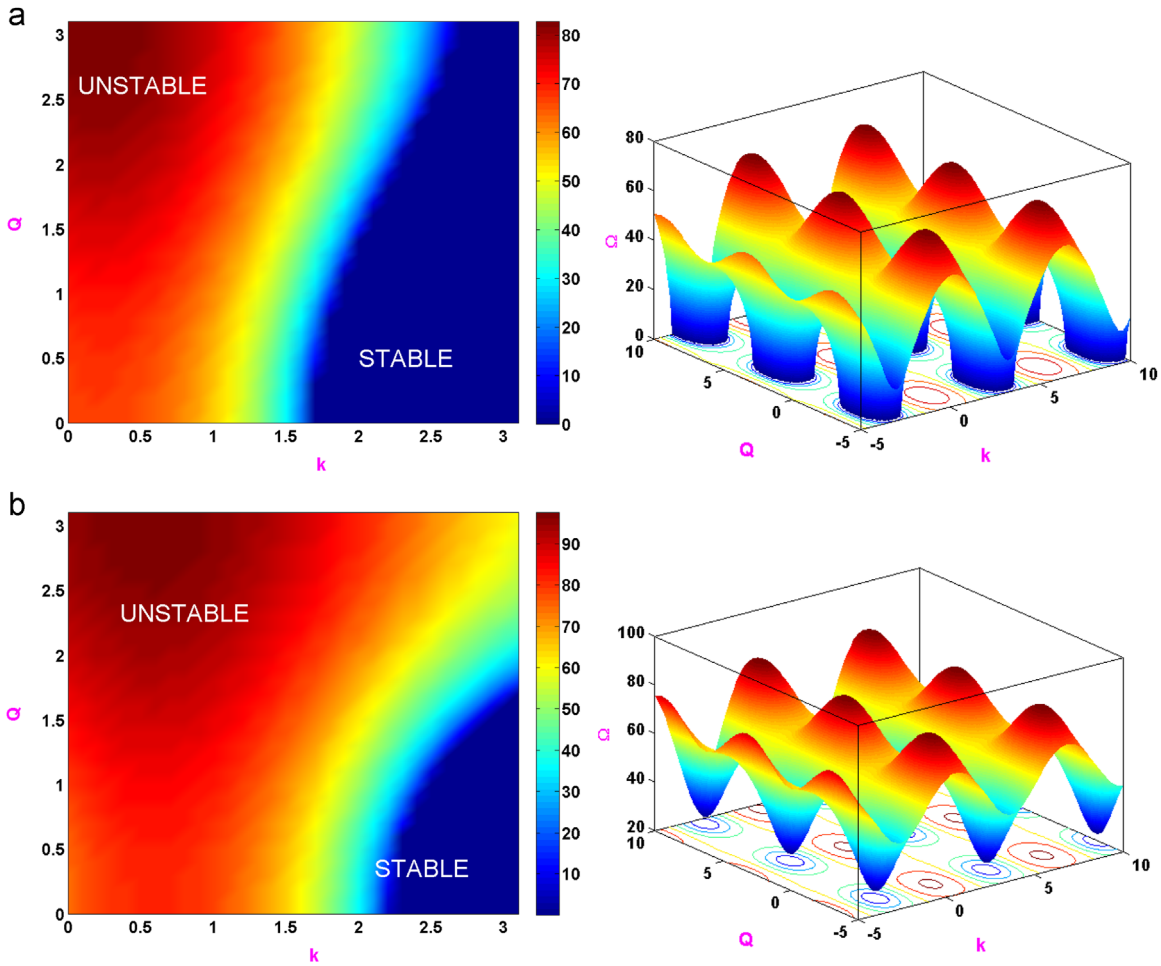

Fig. 4. Left columns: Stability/instability region in the (k, Q) plane. Right columns: MI gain profile for (a) $\beta=0.2$, (b) $\beta=1.2$ and on all plots $\alpha=0.5$, $\gamma=0.85$. (For interpretation of the references to color in this figure caption, the reader is referred to the web version of this paper.)

bands, and the simulations confirm the prediction of instability when a modulated wave moves in the spin chain with a nonvanishing imaginary part of the frequency of the modulated wave. We carried out the longer-time dynamical simulations for $t=900$ units for the values of coupling parameters $\alpha=0.41$, $\beta=1.41$ and $\gamma=0.38$ as shown in Fig. 6(c). From all these figures, we notice that the presence of not only the principal $k\pm Q$ satellite modulations also the other higher harmonics $2Q$, $3Q\cdots k\pm 2Q$ display an appreciable exponential blowing up. From these figures, it is also revealed that the amplitude of most of the Fourier components of the various combination modes initially increases at a small rate of instability and notably the $3Q$ modulation induces a higher instability in the system thus driving the system into a chaotic regime at longer time scales with its wavevector falling well in an instability domain.

5. Localization of energy

It has been demonstrated by Lai and Sievers [61,28,57] that in an antiferromagnetic spin chain, a delocalized state in Fourier space can either be a localized state or a delocalized state in the corresponding real space, depending on the relative phases between Fourier components. The time evolution in Fourier space alone does not tell us the complete process of energy distribution. However, it is generally believed that the system will finally reach equipartition of energy in a sufficiently long time since entropy should grow during the long time evolution of the system.

Generally, one of the major consequences of the MI is the creation of localized excitations from spatially extended spin excitations in a ferromagnetic lattice. In this section, we investigate how the energy initially concentrated in few modes is redistributed in a weak ferromagnetic chain of 256 spins. As predicted by many authors [48,69], MI is a first step towards energy localization in nonlinear lattices. This MI induced energy localization has been proposed to be the mechanism responsible for the formation of intrinsic localization. The normalized energy density distribution is represented as

$$e(n,t)=\sum_{n}\Bigg[2(u_{n+1}^{*}+u_{n-1}^{*})u_n+4\epsilon^2\gamma|u_n|^4+2\alpha\epsilon^2(|u_{n+1}|^2+|u_{n-1}|^2)|u_n|^2+\frac{\epsilon^2}{4}\Big((u_{n+1}+u_{n-1})|u_n|^2u_n^{*}+(u_{n+1}^{*}+u_{n-1}^{*})|u_n|^2u_n\Big)+i\beta\Big[(u_{n+1}^{*}-u_{n-1}^{*})u_n-\frac{\epsilon^2}{4}\Big((u_{n+1}-u_{n-1})|u_n|^2u_n^{*}+(u_{n+1}^{*}-u_{n-1}^{*})|u_n|^2u_n\Big)\Big]\Bigg]. \quad (13)$$

We perform the MD simulations to compute the evolution of energy density equation (13) and analyse the play role of the exchange interaction parameters on the formation of DBs. In the previous section, we addressed the study of a linear wave under modulation with its wave vector falling in an unstable region. As already evidenced some higher harmonics will inevitably exhibit the exponential

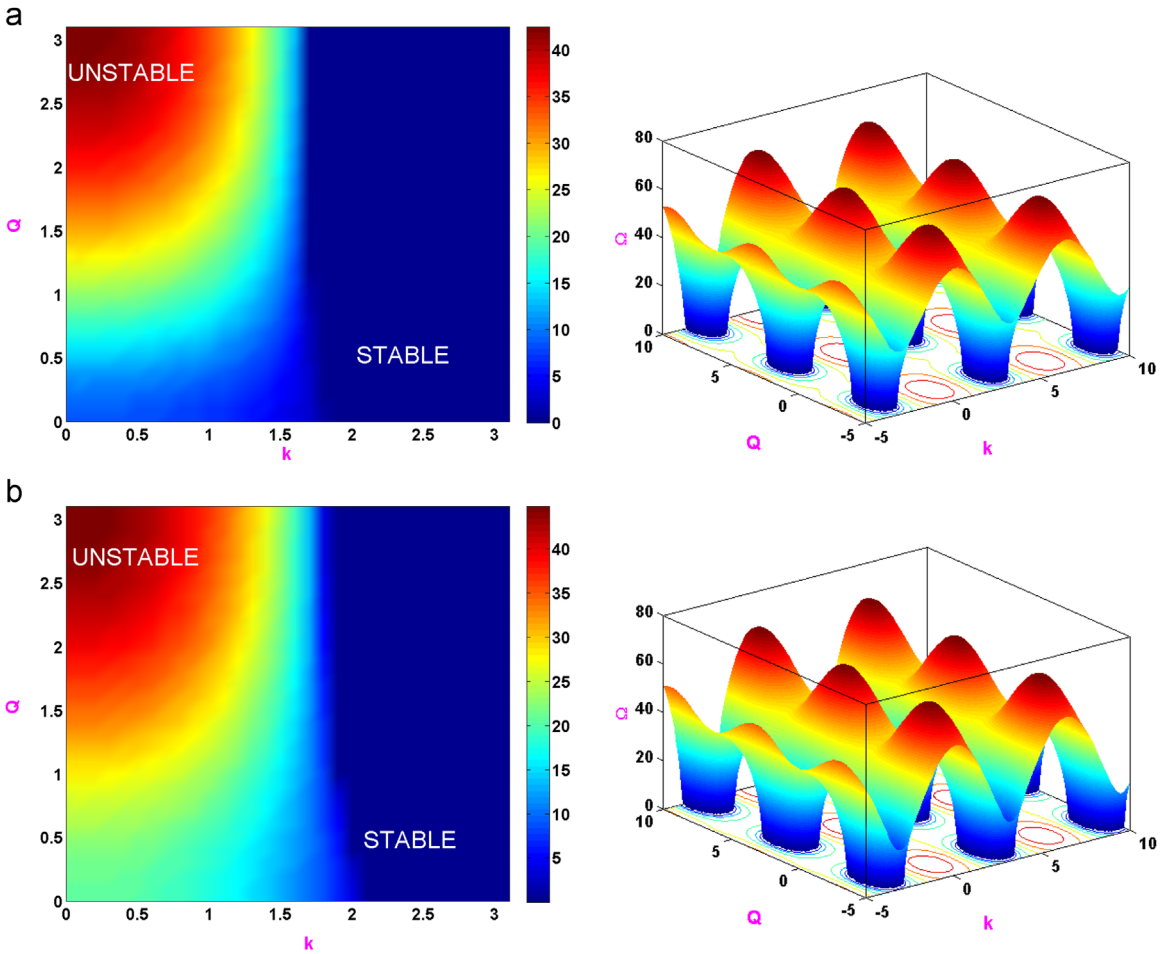

Fig. 5. Left columns: Stability/instability region in the (k, Q) plane. Right columns: MI gain profile for (a) $\gamma=0.2$, (b) $\gamma=1.0$ and on all plots $\alpha=0.5$, $\beta=0.2$. (For interpretation of the references to color in this figure caption, the reader is referred to the web version of this paper.)

growth and finally this instability will destroy completely the coherence of initial condition. This is exactly what we found and what we present in Fig. 7. In Fig. 7, we plot the temporal evolution of the energy density for various values of the DM interaction parameter to analyse the effect of weak ferromagnetism and the associated spin canting on the localization of energy phenomenon and subsequently on the formation of long-lived discrete breather modes. In the figures, at the beginning, i.e., at the bottom of the panel, the whole chain is grey and coherent which corresponds to an equipartition of the energy through all the sites. The initial uniformly distributed energy becomes localized as the instability develops. After a small delay of about 18 periods of time, the initial linear wave breaks up and a number of localized excitations are created and appear to be trapped by the discreteness of the lattice. Among these localized excitations with varying amount of energy, only a few localized excitations move as discrete breathers and interact with each others. The horizontal axis indicates the position along the chain and the vertical axis corresponds to the time. The gray scale goes from $E_n=0$ (dark) to the maximum E_n (white). In Figs. 7a(i)–(iii), as an influence of the parameter α related to the exchange anisotropy along the easy axis of magnetization, it is illustrated that the nonlinear development of the MI in the weak ferromagnetic spin lattice is set up more quickly for the DM interaction parameter $\beta=0.4$. Certainly, the parameter β determines the life time of the discrete breather modes which appears to last for a range of time scale sufficiently long in few cases. In the panels shown in Fig. 7a(i), the parameters take the values of $\alpha=1.41$, $\beta=0.4$ and $\gamma=0.38$, which display the evolution of energy along the chain, the horizontal axis indicates the lattice position along the chain and the vertical axis corresponds to the time. In the panel, the dark area refers to the zero or minimum energy and the brighter lines refers to the maximum energy. In Figs. 7a(i)–(iii), it is obviously understood that upon an increase in the parameter α, the MI sets in earlier, which ultimately kills many short lived DBs and the DBs with maximum energy is more persistent and survive for a sufficiently longer time. A similar trend can be observed in Fig. 7 (b) and for the value of$\beta=0.4$, $\alpha=1.41$ though the instability break up occurs more early than the previous one, it allows the DBs to interact much with each other. Surprisingly, the temporal evolution of energy density for the case $\alpha=3.0$ leads to the generation of incoherent DBs and the subsequent trapping of the same in the spin lattices as shown in Fig. 7b(iii).

The co-existence of nonlinearity and discreteness in the weak ferromagnetic chain supports the existence of ILMs or DBs that oscillate for long time in a localized region of space. This existence has been rigorously proved [57,62] and they can be constructed using standard numerical algorithms [63–70]. We aim to construct DBs numerically in the framework of the one dimensional model for weak ferromagnetic spin chains. The computational tools for studying DB properties are confined to the case of a finite lattice size. We construct the DBs in a discrete weak ferromagnetic chain through numerical simulations using Newton–Raphson scheme. According to the simplest version of this method, one looks for the stationary wave solutions in the form of $u_n = u_n e^{i\Lambda t}$, where Λ is the nonlinearity induced shift in the propagation constant. Our

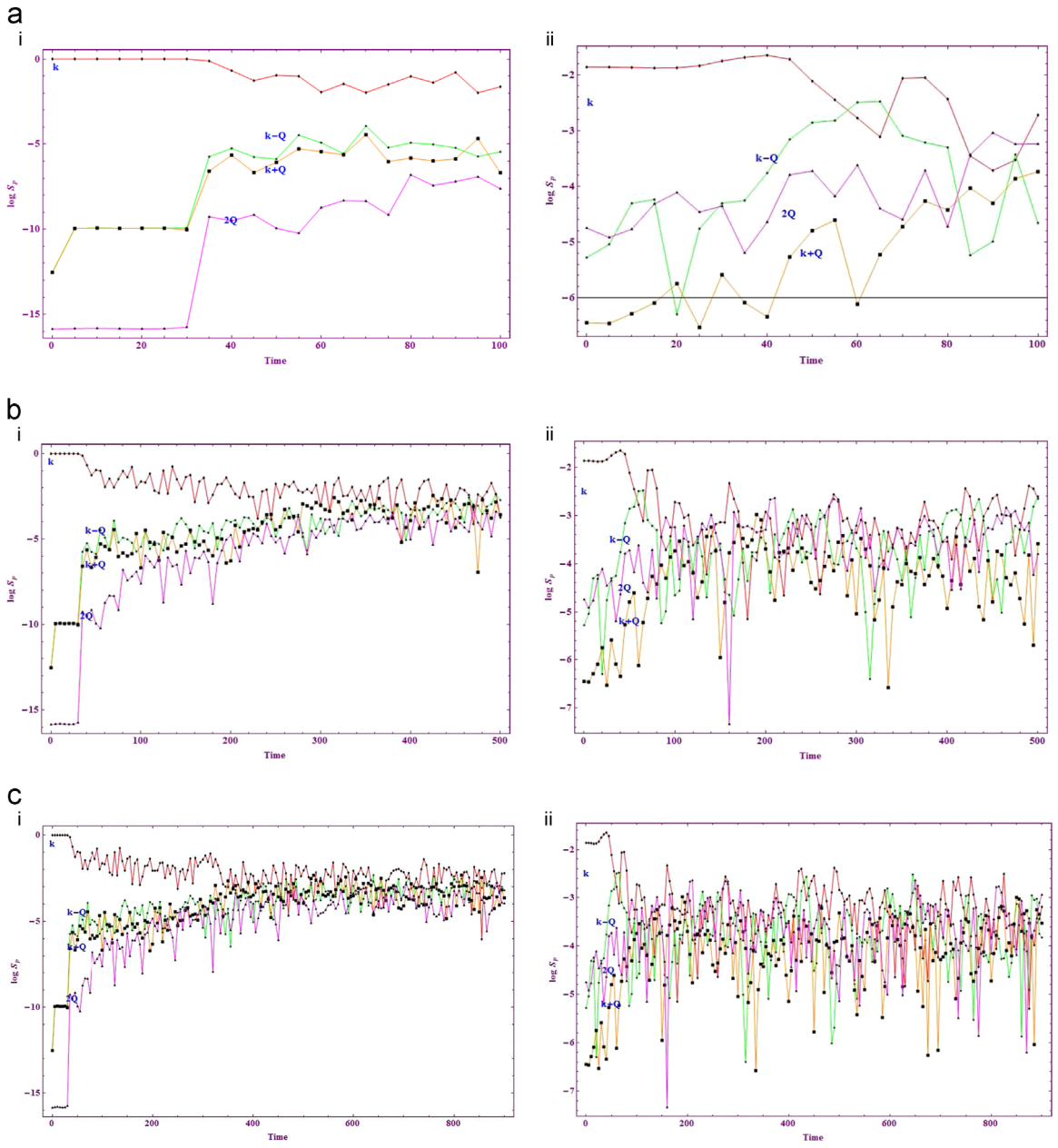

Fig. 6. Time evolution of the Fourier components and complete spatial Fourier spectrum of the wave for (a) $t=100$, (i) k = 0, Q = $\pi/2$ (ii) k = $\pi/3$, Q = $5\pi/6$. (b) $t=500$, (i) k = 0, Q = $\pi/2$ (ii) k = $\pi/3$, Q = $5\pi/6$. and (c) $t=900$, $\alpha=0.41$, $\beta=1.41$, and $\gamma=0.38$, (i) k = 0, Q = $\pi/2$ (ii) k = $\pi/3$, Q = $5\pi/6$. on all plots.

numerical calculation is made at $n=45$ units of spin and we seek the localized modes in the form of DBs, by varying the values of the exchange interaction coupling parameters. Figs. 8a(i) and (ii) display the snapshots of oscillating DBs centred at different sites in weak ferromagnetic spin chain for various values of α the bilinear exchange anisotropic coupling parameter. From the figures, it is manifested that the exchange anisotropic parameter α influences on the amplitude and width of the existing bulk multisite breather modes. Upon tuning the initial conditions appropriately, we obtain three-site symmetric bulk DB localized over four lattice sites, with an amplitude of 1.18 when there is no anisotropic exchange (i.e.,$J_2 = 0$, $\alpha = 0$) with the values of parameters $\beta=0.1$ and $\gamma=0.1$, as shown in Fig. 8a(i). On the contrary, after an introduction of the exchange anisotropy $J_2 \neq 0$, the amplitude of the DB shoots up to 10 times rather the previous one, as shown in Fig. 8a(ii) and widens the width of DB with more number of lattice sites participating in the motion. In Fig. 8(b), the effect of DM interaction on the formation of DBs is analysed. In the absence of DM interaction $\beta=0$, we obtain a single-site symmetric DB, centred at $n=23$ as shown in Fig. 8b(i). However, when the DM interaction parameter is slowly enhanced from 0 to 0.02, the amplitude of the DB is increased slightly. Upon further increasing the DM interaction parameter β, we observe a remarkable increase in the amplitude of the DB and it leads to the participation of more number of lattice sites on the formation of localized DB centred at $n=23$ as shown in Fig. 8b(ii). It is evident from the plots that the amplitude of the DB is directly proportional to the strength of the DM interaction. The stronger of the DM interaction is, the wider and taller the DB appears in the system. From the snapshots it has been realized that in the weak ferromagnetic chain, the degree of spin canting as a result of weak antisymmetric coupling modulates the amplitude of the DB more appreciably. Thus the presence of DM

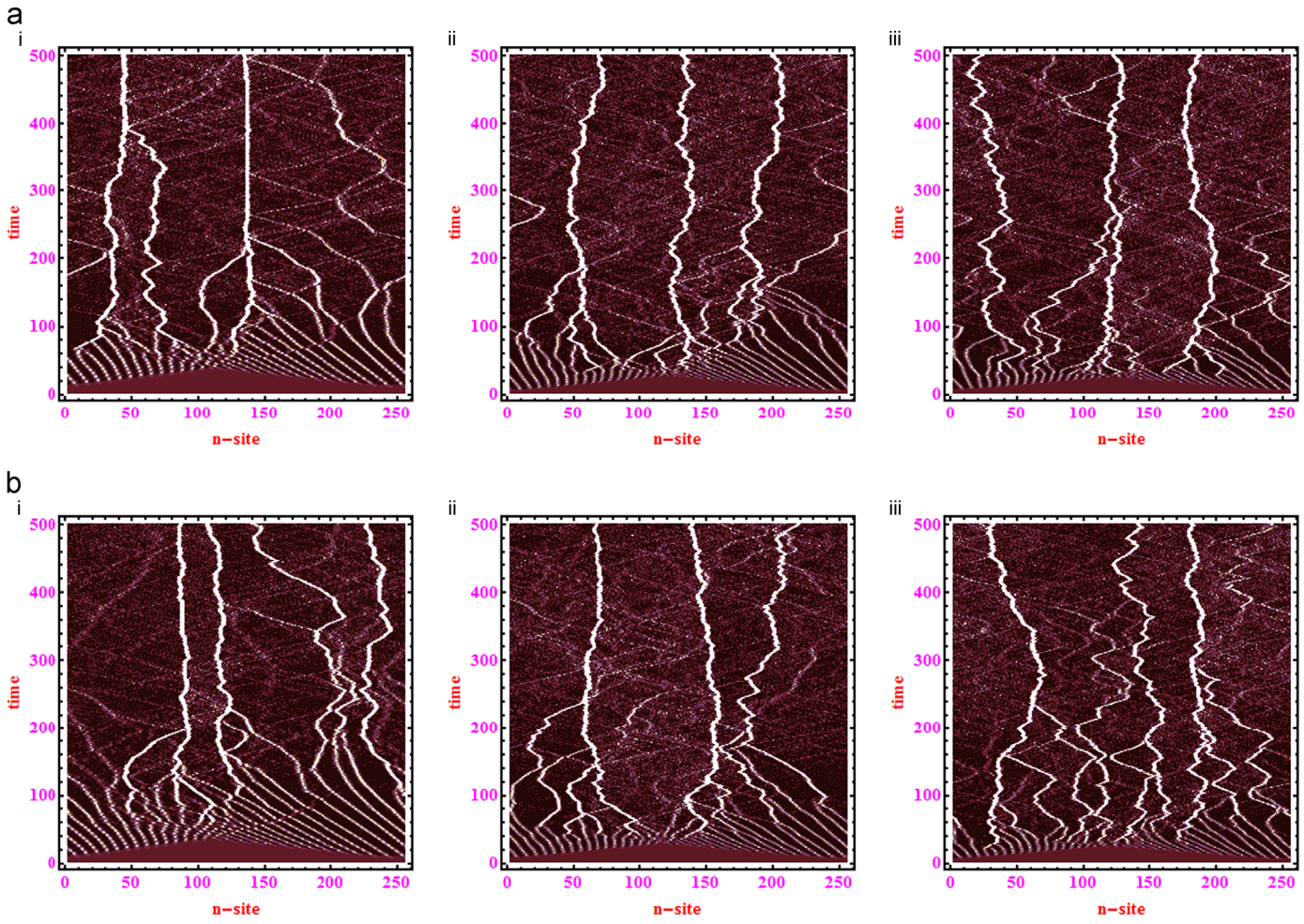

Fig. 7. Evolution of the energy density along the chain. The parameters are γ=0.38 for (a) β=0.4, (i) $\alpha = 1.41$ (ii) $\alpha = 2.4$ (iii) $\alpha = 3.0$ and (b) β=0.8, (i) $\alpha = 1.41$ (ii) $\alpha = 2.4$ (iii) $\alpha = 3.0$.

interaction in a ferromagnetic spin lattice influences the properties of nonlinear excitations even at the nano-scale length as shown in Figs. 8b(i) and (ii). Thus in a weak ferromagnetic spin chain, it is demonstrated that both discreteness and strong antisymmetric coupling is essential for the creation of long-lived localized excitations or DBs.

6. Stability analysis of DBs

We would like to analyse the linear stability of DBs by introducing the following expansion:

$$u_n(t) = (\phi_n + \delta\phi_n(t))e^{i(nk+\omega t)}, \tag{14}$$

where ϕ_n designates the unperturbed amplitude and $\delta\phi_n(t)$ is a small perturbation. Upon substituting Eq. (14) in Eq. (4), further, by splitting the perturbation $\delta\phi_n$ into real part δa_n and imaginary part δb_n, i.e., $\delta\phi_n = \delta a_n + \mathrm{i}\ \delta b_n$ and introducing the two real vectors

$$\delta A_n = \{\delta a_n\} \quad \text{and} \quad \delta B_n = \{\delta b_n\},$$

and the two real matrices $A = \{A_{nm}\}$ and $B = \{B_{nm}\}$, we elucidate the following eigenvalue problem:

$$\begin{pmatrix} \delta\dot{A} \\ \delta\dot{B} \end{pmatrix} = \begin{pmatrix} M_1 M_3 \\ M_2 M_4 \end{pmatrix} \begin{pmatrix} \delta A \\ \delta B \end{pmatrix} = \hat{M} \begin{pmatrix} \delta A \\ \delta B \end{pmatrix}, \tag{15}$$

with

$$\begin{aligned}(M_1)_{nm} = &\Bigg[\frac{\epsilon^2}{4}\{2\phi_n(\phi^*_{n+1} - \phi^*_{n-1})\sin(k) - 2\phi_n(\phi_{n+1} + \phi_{n-1})\sin(k)\} \\ &+ \frac{\beta\epsilon^2}{4}\{\phi_n(\phi_{n+1} + \phi_{n-1})\cos(k) + 2\phi^*_n\cos(k) \\ &+ 2\phi_n(\phi^*_{n-1} - \phi^*_{n+1})\cos(k)\}\Bigg]\delta_{n,m} + \Bigg[2\sin(k) - \frac{\epsilon^2}{4}\{2|\phi_n|^2\sin(k) \\ &+ \phi_n^2\sin(k)\} - \beta\Bigg\{\cos(k) + \frac{\epsilon^2}{4}\{2|\phi_n|^2\cos(k) \\ &+ \phi_n^2\cos(k)\}\Bigg\}\Bigg](\delta_{n,m+1} - \delta_{n,m-1}) + \Bigg[\frac{\beta\epsilon^2}{4}\{2|\phi_{n+1}|^2\cos(k) \\ &+ \phi_{n+1}^2\cos(k)\} - \frac{\epsilon^2}{4}\{2|\phi_{n+1}|^2\sin(k) + \phi_{n+1}^2\sin(k)\}\Bigg]\delta_{n,m+1} \\ &+ \Bigg[\frac{\beta\epsilon^2}{4}\{2|\phi_{n-1}|^2\cos(k) + \phi_{n-1}^2\cos(k)\} - \frac{\epsilon^2}{4}\{2|\phi_{n-1}|^2\sin(k) \\ &+ \phi_{n-1}^2\sin(k)\}\Bigg]\delta_{n,m-1},\end{aligned}$$

$$
\begin{aligned}
(M_2)_{nm} = \Bigg[& \omega + 4\epsilon^2\gamma\{2|\phi_n|^2 + \phi_n^2\} + 2\alpha\epsilon^2(|\phi_{n+1}|^2 + |\phi_{n-1}|^2) \\
& - \frac{\epsilon^2}{4}\{2\phi_n^* \cos(k) + 2\phi_n(\phi_{n+1} + \phi_{n-1})\cos(k) \\
& + 2\phi_n(\phi_{n+1}^* + \phi_{n-1}^*)\cos(k)\} \\
& + \frac{\beta\epsilon^2}{4}\{2\phi_n(\phi_{n+1} - \phi_{n-1})\sin(k) + 4\phi_n^* \sin(k) \\
& - 2\phi_n(\phi_{n+1}^* + \phi_{n-1}^*)\sin(k)\}\Bigg]\delta_{n,m} \\
& + \Bigg[2\cos(k) - \frac{\epsilon^2}{4}\{2|\phi_n|^2\cos(k) + \phi_n^2\cos(k)\} \\
& + \beta\left\{\sin(k) + \frac{\epsilon^2}{4}\{2|\phi_n|^2\sin(k) - \phi_n^2\sin(k)\}\right\}\Bigg](\delta_{n,m+1} \\
& + \delta_{n,m-1}) \\
& + \Bigg[2\alpha\epsilon^2(\phi_{n+1}\phi_n + \phi_{n+1}^*\phi_n) + \frac{\beta\epsilon^2}{4}\{2|\phi_{n+1}|^2\sin(k) \\
& + \phi_{n+1}^2\sin(k)\} - \frac{\epsilon^2}{4}\{2|\phi_{n+1}|^2\cos(k) + \phi_{n+1}^2\cos(k)\}\Bigg]\delta_{n,m+1} \\
& + \Bigg[2\alpha\epsilon^2(\phi_{n-1}\phi_n + \phi_{n-1}^*\phi_n) + \frac{\beta\epsilon^2}{4}\{2|\phi_{n-1}|^2\sin(k) \\
& + \phi_{n-1}^2\sin(k)\} - \frac{\epsilon^2}{4}\{2|\phi_{n-1}|^2\cos(k) + \phi_{n-1}^2\cos(k)\}\Bigg]\delta_{n,m-1},
\end{aligned}
$$

$$
\begin{aligned}
(M_3)_{nm} = \Bigg[& \omega + 4\epsilon^2\gamma\{2|\phi_n|^2 - \phi_n^2\} + 2\alpha\epsilon^2(|\phi_{n+1}|^2 + |\phi_{n-1}|^2) \\
& - \frac{\epsilon^2}{4}\{4\phi_n^* \cos(k) - 2\phi_n(\phi_{n+1} + \phi_{n-1})\cos(k) \\
& + 2\phi_n(\phi_{n+1}^* + \phi_{n-1}^*)\cos(k)\} \\
& + \frac{\beta\epsilon^2}{4}\{2\phi_n(\phi_{n+1} - \phi_{n-1})\sin(k) + 4\phi_n^* \sin(k) \\
& - 2\phi_n(\phi_{n+1}^* - \phi_{n-1}^*)\sin(k)\}\Bigg]\delta_{n,m} \\
& + \Bigg[2\cos(k) - \frac{\epsilon^2}{4}\{2|\phi_n|^2\cos(k) - \phi_n^2\cos(k)\} \\
& + \beta\left\{\sin(k) + \frac{\epsilon^2}{4}\{|\phi_n|^2\sin(k) + \phi_n^2\sin(k)\}\right\}\Bigg](\delta_{n,m+1} \\
& + \delta_{n,m-1}) \\
& + \Bigg[2\alpha\epsilon^2(\phi_{n+1}^*\phi_n - \phi_{n+1}\phi_n) - \frac{\beta\epsilon^2}{4}\{2|\phi_{n+1}|^2\sin(k) \\
& + \phi_{n+1}^2\sin(k)\} - \frac{\epsilon^2}{4}\{2|\phi_{n+1}|^2\cos(k) - \phi_{n+1}^2\cos(k)\}\Bigg]\delta_{n,m+1} \\
& + \Bigg[2\alpha\epsilon^2(\phi_{n-1}^*\phi_n - \phi_{n+1}\phi_n) + \frac{\beta\epsilon^2}{4}\{2|\phi_{n-1}|^2\sin(k) \\
& - \phi_{n-1}^2\sin(k)\} - \frac{\epsilon^2}{4}\{2|\phi_{n-1}|^2\cos(k) - \phi_{n-1}^2\cos(k)\}\Bigg]\delta_{n,m-1},
\end{aligned}
$$

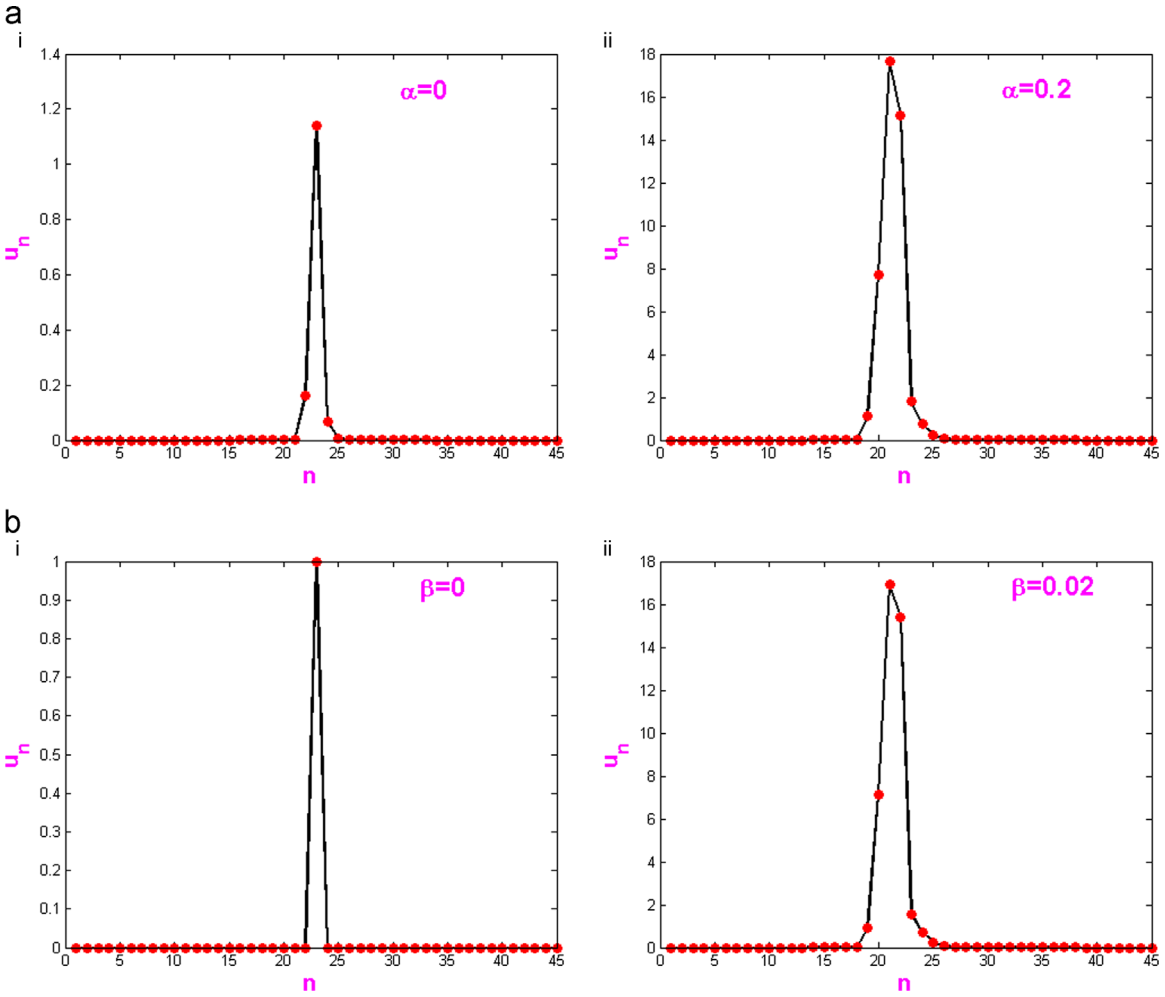

Fig. 8. Snapshots of breather profile at $\Lambda=1.8$ for (a) $\beta=0.1$, (b) $\alpha=1.5$, and $\gamma=0.1$ on all plots.

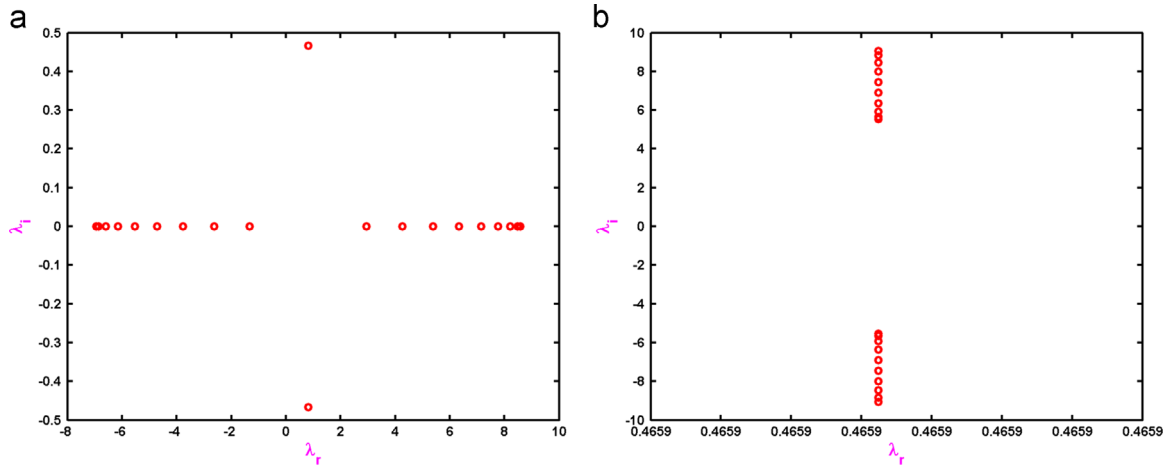

Fig. 9. Eigenvalue spectrum of the DBs for the choice of the parameters β=0.66 and γ=0.450. (a) α=0.0983. (b) α=0.172.

$$
\begin{aligned}
(M_4)_{nm} = \Bigg[& -\frac{\epsilon^2}{4}\{2\phi_n(\phi^*_{n+1}+\phi^*_{n-1})\sin(k) + 2\phi_n(\phi_{n+1}+\phi_{n-1})\sin(k)\} \\
& + \frac{\beta\epsilon^2}{4}\{\phi_n(\phi_{n+1}+\phi_{n-1})\cos(k) - 4\phi^*_n\cos(k) \\
& + 4\phi_n(\phi^*_{n+1}-\phi^*_{n-1})\cos(k)\}\Bigg]\delta_{n,m} + \Bigg[2\sin(k) - \frac{\epsilon^2}{4}\{2|\phi_n|^2\sin(k) \\
& + \phi_n^2\sin(k)\} - \beta\Bigg\{\cos(k) - \frac{\epsilon^2}{4}\{2|\phi_n|^2\cos(k) \\
& + \phi_n^2\cos(k)\}\Bigg\}\Bigg](\delta_{n,m+1}-\delta_{n,m-1}) - \Bigg[\frac{\beta\epsilon^2}{4}\{2|\phi_{n+1}|^2\cos(k) \\
& - \phi_{n+1}^2\cos(k)\} - \frac{\epsilon^2}{4}\{2|\phi_{n+1}|^2\sin(k) + \phi_{n+1}^2\sin(k)\}\Bigg]\delta_{n,m+1} \\
& + \Bigg[\frac{\beta\epsilon^2}{4}\{2|\phi_{n-1}|^2\cos(k) + \phi_{n-1}^2\cos(k)\} \\
& + \frac{\epsilon^2}{4}\{\phi_{n-1}^2\sin(k) - 2|\phi_{n-1}|^2\sin(k)\}\Bigg]\delta_{n,m-1}.
\end{aligned}
$$

The DBs are linearly stable if and only if the matrix M has all its eigenvalues on the imaginary axis; otherwise the DBs are unstable [71–73]. In our stability analysis, the eigenvalue spectrum always contains eigenvalues which are zero. This eigenvalue corresponds to the (ς) translational invariance and to the invariance of the solution to a constant phase factor, respectively. Figs. 9(a) and (b) portray the eigenvalue spectrum in the spectral plane (λ_i, λ_r) for the parametric choices $\alpha = 0.0983$, $\gamma = 0.450$ and $\beta = 0.66$. As shown in Figs. 9(a) and (b), it could be observed that when $\alpha < 0.172$, all the eigenvalues are occupying both the real and imaginary axes of the spectral plane exploring the instability window and once $\alpha = 0.172$, suddenly all the eigenvalues at the real axis are vanished and an abrupt gathering of eigenvalues on the imaginary axis could be manifested from Fig. 9(b), leading to a platform for stable localized modes. These figures expose the impact of the exchange anisotropy parameter α on the stability window.

7. Conclusions

We have investigated the nonlinear dynamics of a discrete weak ferromagnetic chain with on-site easy-axis anisotropy due to crystal field effect. The quasiclassical equation of motion for the nonlinear evolution of the Heisenberg spin system is obtained by employing the boson mappings of spin operators via Holstein–Primakoff transformation and Glauber's coherent-state representation. We performed a systematic modulational instability analysis both analytically in the framework of linear stability analysis and numerically by means of molecular dynamics simulations. The numerical simulations also enabled us to examine the long-time evolution of modulational instabilities and demonstrate the possibility of the formation of localized structures. We investigate the properties of modulational instabilities and subsequent formation of discrete breathers for the energy exchange parameters of interest and we check that there is a systematic tendency to favour the growth of the larger DB excitations with higher amplitudes. We analysed the stability/instability of DBs using Fourier collocation method. These results allow us to draw conclusions that the spin–orbit induced Dzyaloshinsky–Moriya interaction and the anisotropy have profound impact on the DB excitations and the antisymmetric nature of the canted ferromagnetic medium supports the long-lived nano-scale localized excitations in the form of single-site DBs.

Acknowledgements

L.K. gratefully acknowledges the financial support by UGC (F.30-1/2013 (SA-II)/RA-2012-14-NEW-SC-TAM-3228) in the form of a research award, NBHM (2/48(9)/2011/-R&D II/1223) in the form of a major research project, DAE-BRNS (2009/20/37/7/BRNS/1819), India in the form of a Young Scientist Research Award, and ICTP, Italy in the form of a Regular Associateship. E.P. gratefully acknowledges Periyar University for providing the University Research Fellowship. R.A. Vicencio acknowledges supports from Fondecyt Grant no. 1151444 and Programa ICM Grant no. RC-130001.

References

[1] A. Mboussi Nkomidio, S. Noubissie, P. Woafo, Dynamics of arrays of legs powered by a discrete electrical model of nerve, Phys. Lett. A 378 (2014) 857–862.
[2] M. Peyrard, M.D. Kruskal, Kink dynamics in the highly discrete sine-Gordon system, Physica D 14 (1984) 88–102.
[3] M. Peyrard, St. Pnevmatikos, N. Flytzanis, Discreteness effects on non-topological kink soliton dynamics in nonlinear lattices, Physica D 19 (1986) 268–281.
[4] A.J. Sievers, S. Takeno, Intrinsic localized modes in anharmonic crystals, Phys. Rev. Lett. 61 (1998) 970.
[5] J. Pouget, S. Aubry, A.R. Bishop, P.S. Lomdahi, Transverse wall instabilities on a driven, damped two-dimensional lattice system, Phys. Rev. B 39 (1989) 9500.
[6] R. Scharf, A.R. Bishop, Properties of the nonlinear Schrödinger equation on a Lattice, Phys. Rev. A 43 (1991) 6535.

[7] R. Lai, A.J. Sievers, Phase problem associated with the determination of the longitudinal shape of a charged particle bunch from its coherent far-IR spectrum, Phys. Rev. E 52 (1995) 4576.
[8] M. Daniel, L. Kavitha, R. Amuda, Soliton spin excitations in an anisotropic Heisenberg ferromagnet with octupole–dipole interaction, Phys. Rev. B 59 (1999) 13774.
[9] M. Daniel, L. Kavitha, Localized spin excitations in an anisotropic Heisenberg ferromagnet with Dzyaloshinsky–Moriya interactions, Phys. Rev. B 63 (2001) 172302.
[10] M. Daniel, L. Kavitha, Magnetization reversal through soliton flip in a biquadratic ferromagnet with varying exchange interactions, Phys. Rev. B 66 (2002) 184433.
[11] L. Kavitha, P. Sathishkumar, D. Gopi, Creation and annihilation of solitons in a ferromagnet with competing nonlinear inhomogeneities, Phys. Scr. 81 (2010) 035404.
[12] M. Daniel, L. Kavitha, Soliton in an anisotropic spin ladder with site and spin-dependent Dzyaloshinsky–Moriya interaction, Phys. Lett. A 295 (2002) 121.
[13] L. Kavitha, M. Daniel, Integrability and soliton in a classical one-dimensional site-dependent biquadratic Heisenberg spin chain and the effect of nonlinear inhomogeneity, J. Phys. A: Math. Gen. 36 (2003) 10471.
[14] L. Kavitha, P. Sathishkumar, M. Saravanan, D. Gopi, Soliton switching in an anisotropic Heisenberg ferromagnetic spin chain with octupole–dipole interaction, Phys. Scr. 83 (2011) 055701.
[15] L. Kavitha, M. Saravanan, B. Srividya, D. Gopi, Breatherlike electromagnetic wave propagation in an antiferromagnetic medium with Dzyaloshinsky–Moriya interaction, Phys. Rev. E 84 (2011) 066608.
[16] L. Kavitha, P. Sathishkumar, D. Gopi, Energy-momentum transport through soliton in a site-dependent ferromagnet, Commun. Nonlinear Sci. Numer. Simul. 16 (2011) 1787.
[17] L. Kavitha, P. Sathishkumar, D. Gopi, Magnetization reversal through flipping solitons under the localized inhomogeneity, J. Phys. A: Math. Theor. 43 (2010) 125201.
[18] L. Kavitha, P. Sathishkumar, D. Gopi, Shape changing soliton in a site-dependent ferromagnet using tanh-function method, Phys. Scr. 79 (2009) 015402.
[19] L. Kavitha, M. Saravanan, N. Akila, S. Bhuvaneswari, D. Gopi, Solitonic transport of energy–momentum in a deformed magnetic medium, Phys. Scr. 85 (2012) 035007.
[20] L. Kavitha, P. Sathishkumar, D. Gopi, Soliton-based logic gates using spin ladder, Commun. Nonlinear Sci. Numer. Simul. 15 (2010) 3900.
[21] G.-F. Zhang, Thermal entanglement and teleportation in a two-qubit Heisenberg chain with Dzyaloshinski–Moriya anisotropic antisymmetric interaction, Phys. Rev. A 75 (2007) 034304.
[22] Y.C. Li, S.S. Li, Quantum critical phenomena in the XY spin chain with the Dzyaloshinski–Moriya interaction, Phys. Rev. A 79 (2009) 032338.
[23] I. Dzyaloshinsky, A thermodynamic theory of "weak" ferromagnetism of antiferromagnetics, J. Phys. Chem. Solids 4 (1958) 241–255.
[24] T. Moriya, Anisotropic superexchange interaction and weak ferromagnetism, Phys. Rev. 120 (1960) 91.
[25] T. Moriya, New mechanism of anisotropic superexchange interaction, Phys. Rev. Lett. 4 (1960) 228.
[26] D. Loss, D.P. DiVincenzo, Quantum computation with quantum dots, Phys. Rev. A 57 (1998) 120.
[27] G. Burkard, D. Loss, D.P. DiVincenzo, Coupled quantum dots as quantum gates, Phys. Rev. B 59 (1999) 2070.
[28] R. Lai, A.J. Sievers, Modulational instability of nonlinear spin waves in easy-axis antiferromagnetic chains, Phys. Rev. B 57 (1998) 3433.
[29] S. Falch, A.V. Gorbach, Discrete breathers—advances in theory and applications, Phys. Rep. 467 (2008) 1.
[30] R.S. MacKay, S. Aubry, Proof of existence of breathers for time-reversible or Hamiltonian networks of weakly coupled oscillators, Nonlinearity 7 (1994) 1623.
[31] J.L. Marin, F. Falo, P.J. Martinez, L.M. Floria, Discrete breathers in dissipative lattices, Phys. Rev. E 63 (2001) 066603.
[32] H.S. Eisenberg, Y. Silberberg, R. Morandotti, A.R. Boyd, J.S. Aitchison, Discrete spatial optical solitons in waveguide arrays, Phys. Rev. Lett. 81 (1998) 3383.
[33] B.I. Swanson, J.A. Brozik, S.P. Love, G.F. Strouse, A.P. Shreve, A.R. Bishop, W.-Z. Wang, M.I. Salkola, Observation of intrinsically localized modes in a discrete low-dimensional materia, Phys. Rev. Lett. 82 (1999) 3288.
[34] F.M. Russell, J.C. Eilbeck, Evidence for moving breathers in a layered crystal insulator at 300 K, Europhys. Lett. 78 (2007) 10004.
[35] U.T. Schwarz, L.Q. English, A.J. Sievers, Experimental generation and observation of intrinsic localized spin wave modes in an antiferromagnet, Phys. Rev. Lett. 83 (1999) 223.
[36] E. Trías, J.J. Mazo, T.P. Orlando, Discrete breathers in nonlinear lattices: experimental detection in a Josephson array, Phys. Rev. Lett. 84 (2000) 741.
[37] M. Sato, A.J. Sievers, Driven localized excitations in the acoustic spectrum of small nonlinear macroscopic and microscopic lattices, Phys. Rev. Lett. 98 (2007) 214101.
[38] M. Sato, B.E. Hubbard, A.J. Sievers, B. Ilic, D.A. Czaplewski, H.G. Craighead, Observation of locked intrinsic localized vibrational modes in a micromechanical oscillator array, Phys. Rev. Lett. 90 (2003) 044102.
[39] A. Xie, L. vander Meer, W. Hoff, R.H. Austin, Long-lived amide I vibrational modes in myoglobin, Phys. Rev. Lett. 84 (2000) 5435.
[40] K.W. Sandusky, J.B. Page, K.E. Schmidt, Stability and motion of intrinsic localized modes in nonlinear periodic lattices, Phys. Rev. B. 46 (1992) 6161.
[41] A.J. Sievers, S. Takeno, Intrinsic localized modes in anharmonic crystals, Phys. Rev. Lett. 61 (1998) 970.
[42] Yu.S. Kivshar, Intrinsic localized modes as solitons with a compact support, Phys. Rev. E 48 (1993) R43 (R).
[43] V.M. Burlakov, S.A. Kiselev, V.N. Pyrkov, Computer simulation of intrinsic localized modes in one-dimensional and two-dimensional anharmonic lattices, Phys. Rev. B 42 (1990) 4921.
[44] J.B. Page, Asymptotic solutions for localized vibrational modes in strongly anharmonic periodic systems, Phys. Rev. B 41 (1991) 7835.
[45] T. Dauxois, M. Peyrard, Energy localization in nonlinear lattices, Phys. Rev. Lett. 70 (1993) 3935.
[46] J.M. Bilbault, P. Marquié, Energy localization in a nonlinear discrete system, Phys. Rev. E 53 (1996) 5403.
[47] S. Aubry, The concept of anti-integrability applied to dynamical systems and to structural and electronic models in condensed matter physics, Physica D 71 (1994) 196.
[48] Yu.S. Kivshar, M. Peyrard, Modulational instabilities in discrete lattices, Phys. Rev. A 46 (1992) 3198.
[49] I. Daumont, T. Dauxois, M. Peyrard, Modulational instability: first step towards energy localization in nonlinear lattices, Nonlinearity 10 (1997) 617.
[50] K.W. Sandusky, J.B. Page, Interrelation between the stability of extended normal modes and the existence of intrinsic localized modes in nonlinear lattices with realistic potentials, Phys. Rev. B 50 (1994) 866.
[51] T.B. Benjamin, J.F. Feir, The disintegration of wave trains on deep water. Part 1. Theory, J. Fluid. Mech. 27 (1967) 417.
[52] P. Marquié, J.M. Bilbault, M. Remoissenet, Generation of envelope and hole solitons in an experimental transmission line, Phys. Rev. E 49 (1994) 828.
[53] P.F. Willis, D.L. Mills, A.D. Boardman, Intrinsic localized spin modes in ferromagnetic chains with on-site anisotropy, Phys. Rev. B 52 (1995) R3828.
[54] S. Takeno, K. Kawasaki, Intrinsic self-localized magnons in one-dimensional antiferromagnets, Phys. Rev. B 45 (1992) 5083.
[55] S. Rakhmanova, D.L. Mills, Nonlinear spin excitations in finite Heisenberg chains, Phys. Rev. B 54 (1996) 9225.
[56] R. Lai, S.A. Kiselev, A.J. Sievers, Intrinsic localized spin-wave modes in antiferromagnetic chains with single-ion easy-axis anisotropy, Phys. Rev. B 54 (1996) R12665 (R).
[57] R. Lai, A.J. Sievers, Identification of an intrinsic localized spin-wave resonance in antiferromagnetic chains with single-ion easy-plane anisotropy, Phys. Rev. B 55 (1997) R11937 (R).
[58] M.I. Molina, R.A. Vicencio, Yu.S. Kivshar, Discrete solitons and nonlinear surface modes in semi-infinite waveguide arrays, Opt. Lett. 31 (2006) 1693.
[59] T. Holstein, H. Primakoff, Field dependence of the intrinsic domain magnetization of a ferromagnet, Phys. Rev. 58 (1940) 1098.
[60] R.J. Glauber, Coherent and incoherent states of the radiation field, Phys. Rev. 131 (1963) 2766.
[61] R. Lai, A.J. Sievers, Nonlinear nanoscale localization of magnetic excitations in atomic lattices, Phys. Rep. 314 (1992) 147.
[62] S. Abdoulkary, A.D. Aboubakar, M. Aboubakar, A. Mohamadou, L. Kavitha, Solitary wave solutions and modulational instability analysis of the nonlinear Schrödinger equation with higher-order nonlinear terms in the left-handed nonlinear transmission lines, Commun. Nonlinear Sci. Numer. Simul. 22 (2015) 1288–1296.
[63] N. Perchikov, O.V. Gendelman, Dynamics and stability of a discrete breather in a harmonically excited chain with vibro-impact on-site potential, Physica D 292–293 (2015) 8–28.
[64] G. James, P.G. Kevrekidis, J. Cuevas, Breathers in oscillator chains with Hertzian interactions, Physica D 251 (2013) 39–59.
[65] L. Kavitha, M. Saravanan, V. Senthilkumar, R. Ravichandran, D. Gopi, Collision of electromagnetic solitons in a weak ferromagnetic medium, J. Magn. Magn. Mater. 355 (2014) 37–50.
[66] E.G. Ekomasov, R.R. Murtazin, O.B. Bogomazova, A.M. Gumerov, One-dimensional dynamics of domain walls in two-layer ferromagnet structure with different parameters of magnetic anisotropy and exchange, J. Magn. Magn. Mater. 339 (2013) 133–137.
[67] N. Boechler, G. Theocharis, S. Job, P.G. Kevrekidis, Mason A. Porter, C. Daraio, Discrete breathers in one-dimensional diatomic granular crystals, Phys. Rev. Lett. 104 (2010) 244302.
[68] L.Z. Khadeeva, S.V. Dmitriev, Discrete breathers in crystals with NaCl structure, Phys. Rev. B 81 (2010) 214306.
[69] L. Kavitha, A. Muniyappan, A. Prabhu, S. Zdravković, S. Jayanthi, D. Gopi, Nano breathers and molecular dynamics simulations in hydrogen-bonded chains, J. Biol. Phys. 39 (2013) 15–35.
[70] D. Toko, R.L. Woulache, C.B. Tabi, L. Kavitha, A. Mohamadou, T.C. Kofane, Breather-like solutions of the twisted DNA with solvent interaction, J. Phys. Chem. Biophys. 3 (2013) 1000112.
[71] L. Kavitha, E. Parasuraman, M. Venkatesh, A. Mohamadou, D. Gopi, Breather-like protonic tunneling in a discrete hydrogen bonded chain with heavy-ionic interactions, Phys. Scr. 87 (2013) 035007 (12 pp.).
[72] L. Kavitha, M. Venkatesh, S. Dhamayanthi, E. Parasuraman, D. Gopi, Optically induced switching of nematic deformations, Phys. Scr. 88 (2013) 065015, 9 pp.
[73] L. Kavitha, M. Venkatesh, M. Saravanan, S. Dhamayanthi, D. Gopi, Breather-like director reorientations in a nematic liquid crystal with nonlocal nonlinearity, Wave Motion 51 (2014) 476–488.